Acta Mech 224, 1943–1955 (2013)
DOI 10.1007/s00707-013-0852-z

Ke Tao · Jun Yao · Zhaoqin Huang

Analysis of the laminar flow in a transition layer with variable permeability between a free-fluid and a porous medium

Received: 1 December 2012 / Revised: 21 February 2013 / Published online: 10 April 2013

Abstract The transport problem in a three-layer channel consisting of a noticeable transition layer sandwiched by a free-fluid region and a homogeneous porous medium is investigated analytically. The heterogeneous transition layer is characterized by the continuous variation of porosity and permeability, which are specifically described by applying two sets of functions. The Brinkman model is employed in the transition layer, and the analytical velocity profile is obtained in terms of the Airy function. Consistency is found between the computation results and the PIV data measured by Goharzadeh et al. (Phys. Fluids 17:057102, 2005). After comparing the estimated permeability variations with the calculated variation, we find the former predicted permeability values are two orders of magnitude larger than the latter ones. The velocity discrepancy in the transition layer is ascribed to the effectiveness of the empirical permeability function: although the well-known Kozeny–Carman formula can precisely predict the permeability of the monodisperse spherical packing bed with constant porosity, it will overestimate the permeability in the transition layer. Then, the exact permeability variation is expressed by an exponential function, and a more general formula is needed to model the gradual change of permeability along the transition layer region.

1 Introduction

Transport phenomena of combined free and porous flow are encountered in numerous industrial, environmental and biological applications, such as the extraction of crude oil from reservoirs, fuel cells, flow through oil filters, nuclear reactors, surface and groundwater flow, contaminant transport from lakes by groundwater, blood flow in a capillary, transfer of therapeutic agents. The corresponding transport mechanism has been intensively investigated in the last decades.

Traditionally, there are two popular ways to model this coupled flow as shown in Fig. 1. The first one is named one-domain approach (ODA), which considers the porous medium as a pseudo-fluid and employs one single equation to describe the fluid flow both in the free-fluid region and in the porous medium. If the interface is an exact surface that separates the homogeneous porous medium and the clear fluid region, then the physical properties are discontinuous, corresponding to the "discontinuous one-domain approach," or a transition layer across which the physical variables encounter possibly strong but nevertheless continuous variations, corresponding to the "continuous one-domain approach" [1]. The modeling is achieved by applying a general transfer equation which is valid everywhere in the domain. If the porous medium is assumed to be homogeneous, this equation takes the form [2]

$$\frac{1}{\varepsilon}\frac{\partial}{\partial t}(\rho\mathbf{u}) + \frac{1}{\varepsilon^2}\nabla\cdot(\rho\mathbf{u}\mathbf{u}) = \rho\mathbf{f} - \nabla p + \mu_{\mathrm{e}}\nabla^2\mathbf{u} - \mu\mathbf{K}^{-1}\cdot\mathbf{u}, \tag{1}$$

K. Tao · J. Yao (✉) · Z. Huang
Department of Reservoir Engineering, School of Petroleum Engineering,
China University of Petroleum (Huadong), 266555 Qingdao, China
E-mail: RCOGFR_UPC@126.com

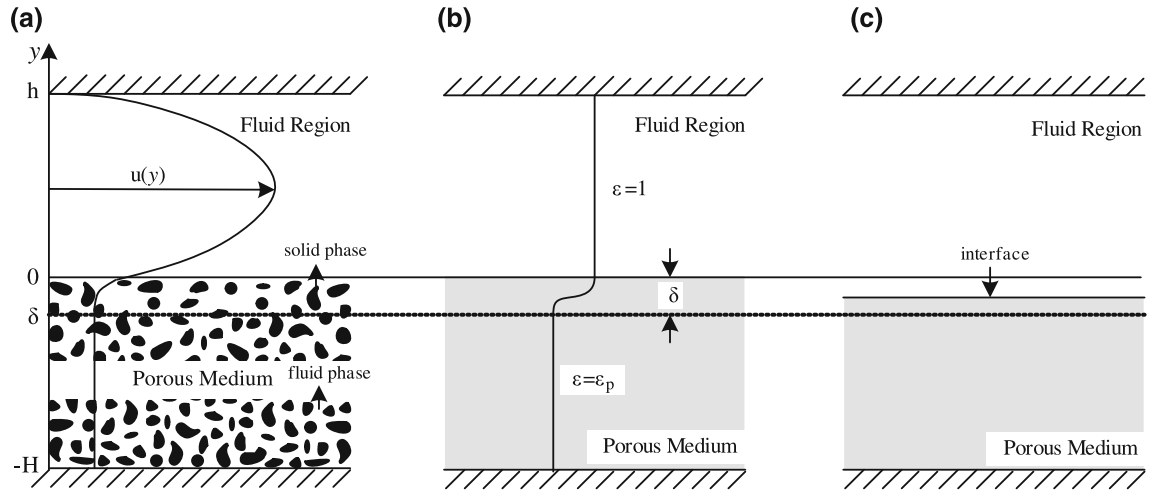

Fig. 1 Distinct descriptions for the flow in the fluid/porous composite structure. **a** Microscopic scale description, **b** one-domain approach configuration, **c** two-domain approach configuration

where ρ signifies the fluid density, **u** is the fluid velocity vector, **f** represents body forces, p is the pressure, **K** is the permeability, ε denotes the porosity, μ_e is the effective viscosity and μ the fluid viscosity. In the free-fluid region, the permeability is infinitely large and Eq. (1) degenerates into the Navier–Stokes equation. For finite values of the permeability of the porous medium, all the terms involving the velocity are formally retained but the Darcy term is predominant; if the permeability is small enough, then the viscous term will be negligible compared to the Darcy term.

Since this formulation avoids explicit interface conditions, it has been extensively used in numerical computation. Good agreement has been obtained in the comparison with experimental results [3–5] using $\mu_e = \mu$ in the calculations. Goyeau et al. [2] used $\mu_e/\mu = 1/\varepsilon_p$ and found that the numerical result using ODA match the analytical result well. The main restriction of the single-domain approach lies in the statement that the Laplacian term may be not valid in low porosity/velocity environments [6].

Based on the domain decomposition method [7], the other approach is called the two-domain approach, using different equations in different subdomains, e.g., Darcy/Brinkman/Forchheimer model in the porous medium and the Navier–Stokes equation in the free-fluid region and coupling them through suitable interface conditions. The work of Beavers and Joseph [8] was among the earlier attempts to study the fluid flow boundary conditions at the interface. They performed an experimental and analytical investigation of fluid flow past a porous material. In order to describe the forced flow in the composite channel, a Stokes flow is considered in the free-fluid region while the momentum transport in the homogeneous porous medium is described by Darcy's law. Due to the different orders of the partial differential equations, an ad hoc slip boundary condition, i.e., BJ condition, is proposed at the interface:

$$\left.\frac{\partial u_x}{\partial y}\right|_{y=0} = \frac{\alpha}{K^{1/2}}\left(u_x|_{y=0} - u_D\right), \tag{2}$$

where u_x denotes the tangential fluid velocity in the channel, u_D is the seepage velocity in the porous medium, K is the permeability and α an empirical dimensionless coefficient. They showed that this boundary condition is consistent with their experiments when the adjustable α ranges from 0.1 to 4. The wide range of α for materials roughly having the same macroscopic averaging properties proves the importance of the interfacial porous structure. Alloui and Vasseur [9] employed this boundary condition to analytically study the stability and natural convection in a system consisting of a horizontal fluid layer over a layer of saturated porous medium. It should be pointed out that Eq. (2) implies a discontinuity in the tangential velocity, i.e., rapid changes of the velocity jumping from that in the fluid region to the porous medium.

In 1995, utilizing a volume averaging method, Ochoa-Tapia and Whitaker [10,11] derived a jump condition: a jump in the effective shear stress, but not in velocity, has been proposed to match the Brinkman–extended Darcy equation with the Stokes equation at the interface, i.e., the OTW condition,

$$\mu_{\mathrm{e}} \left.\frac{\mathrm{d}U_x}{\mathrm{d}y}\right|_{y=0} - \mu \left.\frac{\mathrm{d}u_x}{\mathrm{d}y}\right|_{y=0} = \beta \frac{\mu}{K^{1/2}} \, u_x|_{y=0} \,, \tag{3}$$

where β is a dimensionless adjustable coefficient, it may be positive or negative but must be of order $O(1)$. By adjusting the coefficient β, they achieved a good agreement with the experimental data of Beavers and Joseph. Many studies focused on the estimation of β or obtaining an expression for β which depends on the microstructure of the interface region. Goyeau et al. [2] introduced a continuously varying heterogeneous layer and related β to the continuous spatial variations of the porous structure. Jamet and Chandesris [12] explicitly provided the dependence of β on the internal structure of the transition zone based on matched asymptotic expansions.

However, for the two-domain approach, the solutions can only match the experimental data by adjusting the empirical parameters α or β, which need further physical explanation. To avoid determining the value of β, Duman and Shavit [13] proposed an alternative approach to treat the coupling flow which only needs the easily measured maximum velocity or the flow rate. Besides, Neale and Nader [14] objected to the velocity slip at the interface and stated that the Brinkman equation is mathematically and physically preferable to Darcy's law when considering transition region effects in porous media. Since the Stokes and Brinkman equations are of the same order, continuity of velocity and shear stress should be employed at the interface, which avoids the use of α or β.

When using the two-domain approach, we certainly assume that a sharp interface separates the clear fluid region and the homogeneous porous medium. However, most applications do not have such an abrupt transition, and a gradual change of the geometry marked by the variation of the macroscopic properties (porosity, permeability, etc.) is expected at the intermediate transition layer. Goyeau et al. [2] recalled that an interface is an ideal representation of the transition layer and proclaimed that the information of evolving heterogeneities is important for describing the accurate transport phenomena at the interface region. The thickness of the transition layer is adjusted to fit the interfacial velocity and the flow rate. Following Goyeau et al., Chandesris and Jamet [15] uniformly considered a heterogeneous transition zone in their work. Hill and Straughan [16] discovered two modes of instability corresponding to the fluid and porous layers, respectively, using a homogeneous three-layer structure: a Newton fluid flowing above a Brinkman type porous transition layer, which overlies a layer of Darcy porous medium. Later, Hill [17] further studied the instability of Poiseuille flow and introduced a heterogeneous Brinkman transition layer with continuously varying physical parameters, such as the effective viscosity, the porosity and the permeability which is described by the Carman–Kozeny relationship. Nield and Kuznetsov [18] analytically modeled flow in a three-layer constellation, and Duman and Shavit [19] contributed to the coupling problem by studying the effect of a gradual geometrical change at the interface. Moreover, the flow in the transition layer at a fluid–porous interface is experimentally studied by Goharzadeh et al. [20,22] and Morad and Khalili [21]. The above authors all considered a three-layer composite channel consisting of a noticeable transition layer sandwiched by a porous medium and a fluid, which is the case in this paper.

The objective of the present study is to explore the proper modeling of the variation of the macroscopic parameters in the heterogeneous transition layer between a homogeneous porous medium and a clear fluid. The paper begins with a quantitative comparison between the single-domain model and the two-domain model to address the necessity of specifically modeling the change in macroscopic parameters along the transition region. Then, the appropriate equations for each layer are discussed, and the features of the corresponding properties such as viscosity, porosity and permeability are analyzed. After determining the variation functions of the permeability for the random packs of monodisperse spheres, the exact expressions for the velocity profiles are acquired using Airy, exponential and polynomial functions. The computed velocity profiles are compared with the experimental work of Goharzadeh et al. [22], and the discussion is conducted.

2 Comparison between single- and two-domain approaches

To study the fluid/porous coupling flow, three different description levels [15] are usually considered as shown in Fig. 2. At the microscopic scale, the exact structure of the porous media is depicted and the fluid flows in the free-fluid region and the pores in the porous domain. However, in most practical applications, it is not possible to compute the microscopic flow due to the limitation of the cost and computer capacity. At the mesoscopic scale, the porous domain is represented by two kinds of porous medium: the upper heterogeneous transition layer and the lower homogeneous porous medium; this is the scale covered in this work. However, at the

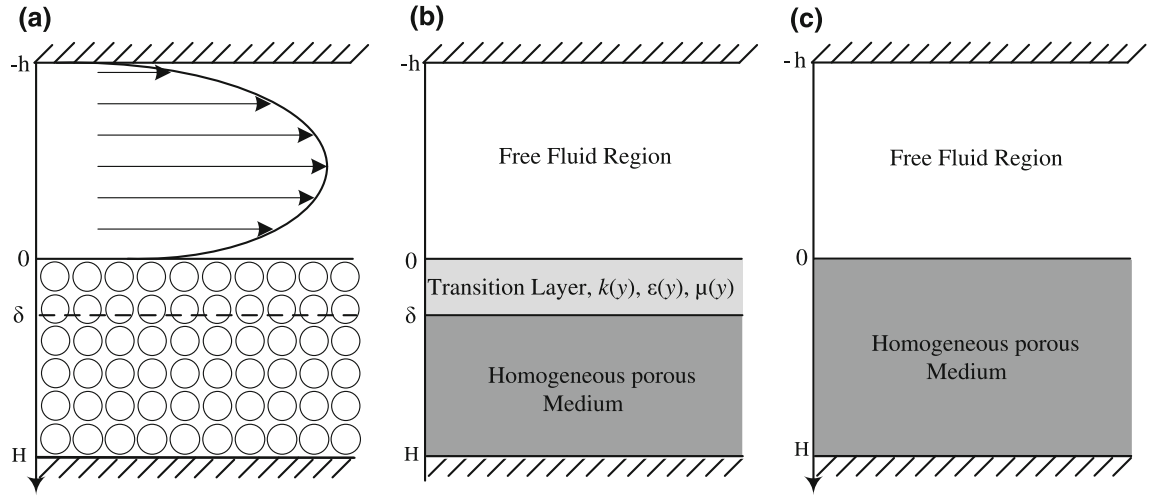

Fig. 2 The three different description scale for the laminar flow in a fluid/porous channel. **a** Microscopic scale description, **b** mesoscopic scale description, **c** macroscopic scale description

macroscopic scale, the composite flow channel is characterized by two homogeneous regions separated by an abrupt interface. The main difference between the latter two descriptions lies in the treatment of the region just beneath the free-fluid region, i.e., the transition layer.

The fundamental configuration considered in this paper consists of three flow domains: the free-fluid region, the intermediate transition layer and the homogeneous porous medium as shown in Fig. 2b. The transition layer is characterized by the continuous variation of macroscopic properties such as the permeability $k(y)$, the porosity $\varepsilon(y)$ and the effective viscosity $\mu(y)$. And we just investigate the stationary incompressible Newton laminar flow in the composite channel where the porous medium is composed of monodisperse spheres.

In this section, a comparison between the single-domain approach and the two-domain approach is conducted to demonstrate the necessity of specifically modeling the change in macroscopic parameters along the transition region. The parameters corresponding to the three-layer model in Fig. 2b are: the transition layer permeability $k_\mathrm{t} = 5 \times 10^{-7}\,\mathrm{m}^2$, porosity $\varepsilon_\mathrm{t} = 0.75$; the homogeneous porous medium permeability $k_\mathrm{p} = 5 \times 10^{-9}\,\mathrm{m}^2$, porosity $\varepsilon_\mathrm{p} = 0.5$; Darcy number $D_a = 5 \times 10^{-3}$, ratio of transition layer thickness to the whole porous medium thickness $\lambda = 0.25$. Here, the permeability in the transition layer is much larger than the lower porous medium layer.

For the single-domain approach, Eq. (1) is employed in the whole channel using specific parameters corresponding to the transition layer and the homogeneous porous medium mentioned above; the numerical results are achieved based on a finite element method. For the two-domain approach, the whole porous domain is treated as one equivalent homogeneous porous medium without considering the exact structure of the transition layer; the Stokes equation is applied in the fluid region and the Brinkman equation in the whole porous domain only using the parameters corresponding to the homogeneous porous medium. After introducing the dimensionless variables $y^* = y/h$, Darcy number $Da = k_\mathrm{p}/h^2, u^* = \mu u/Gh^2$ and the negative pressure gradient $G = -\mathrm{d}p/\mathrm{d}x$, the dimensionless momentum equations and the boundary conditions are given below.

Free-fluid region:

$$\frac{\mathrm{d}^2 u_1}{\mathrm{d}y^2} + 1 = 0 \qquad -h^* \leqq y \leqq 0. \tag{4a}$$

Porous medium:

$$\frac{1}{\varepsilon}\frac{\mathrm{d}^2 u_2}{\mathrm{d}y^2} - \frac{1}{D_a}u_2 + 1 = 0 \qquad 0 \leqq y \leqq H^*. \tag{4b}$$

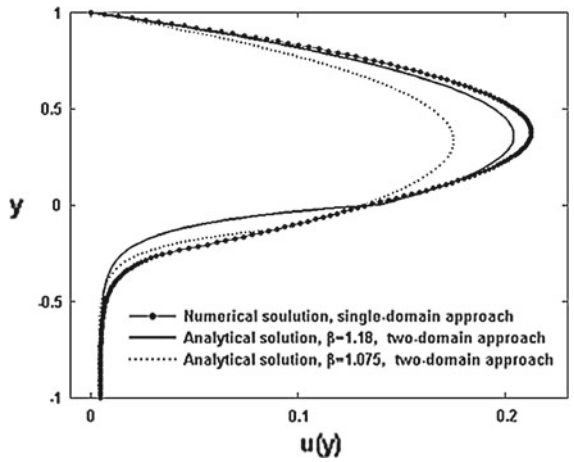

Fig. 3 Comparison between velocity profiles acquired by single-domain approach and two-domain approach with stress jump condition

With boundary conditions:

$$u_1(h^*) = 0, \tag{5a}$$

$$u_2(-H^*) = D_a, \tag{5b}$$

$$u_1(0) = u_2(0), \tag{5c}$$

$$\mu_e \frac{\mathrm{d}u_2}{\mathrm{d}y}\bigg|_{y=0} - \mu \frac{\mathrm{d}u_1}{\mathrm{d}y}\bigg|_{y=0} = \frac{\beta\mu h}{\sqrt{k}} u(0). \tag{5d}$$

Here, h^* and H^* represent the dimensionless value corresponding to h and H. The stress jump boundary condition derived by Ochoa-Tapia and Whitaker is employed.

In Fig. 3, the analytical solutions are achieved with stress jump condition and two different values of β are selected. The analytical solution with $\beta = 1.18$ can better fit the numerical velocity profile than that with $\beta = 1.075$ because the latter one largely underestimates the fluid velocity in the clear fluid region. The discrepancy between the numerical solution and the analytical solution could be explained by the different treatment of the transition region.

The two-domain analytical approach implicitly includes the structure of the specific interfacial region in the ad hoc adjustable dimensionless jump coefficient β; however, the numerical single-domain approach explicitly considers the geometry of the interfacial region by introducing a transition layer. Therefore, although the two-domain approach may predict the velocity profile precisely in the clear fluid channel with specific jump coefficient β, it cannot successfully estimate the velocity distribution in the porous medium. So the two-domain approach is questionable without considering the specific change of the macroscopic properties in the transition layer. Besides, the ambiguity in choosing the suitable value for β further weakens the effectiveness of the stress jump condition. In the following analysis, the shear stress continuity condition will be employed.

Through the above discussion, we conclude that it is necessary to specifically model the macroscopic parameters along the transition region, especially a noticeable transition layer as studied in this work. In the next section, we analytically model the non-homogeneous transition layer taking into account the gradual change of the porosity and permeability.

3 Mathematical model

3.1 Mathematical formulation

The Stokes equation is used in the free-fluid region with fluid viscosity μ_1:

$$-\frac{\mathrm{d}p}{\mathrm{d}x} + \mu_1 \frac{\mathrm{d}^2 u_1}{\mathrm{d}y^2} = 0 \qquad -h \leqq y \leqq 0. \tag{6a}$$

Darcy's law cannot model the penetration of the velocity into the porous medium. In the transition layer, the Brinkman equation considering variable permeability is used and μ_2 is the effective viscosity in the transition layer:

$$-\frac{\mathrm{d}p}{\mathrm{d}x}+\mu_2\frac{\mathrm{d}^2u_2}{\mathrm{d}y^2}-\frac{\mu_1}{k(y)}u_2=0 \qquad 0\leqq y\leqq\delta. \tag{6b}$$

The Brinkman model with constant permeability is employed in the homogeneous porous medium, and μ_3 is the effective viscosity in the homogeneous porous medium:

$$-\frac{\mathrm{d}p}{\mathrm{d}x}+\mu_3\frac{\mathrm{d}^2u_2}{\mathrm{d}y^2}-\frac{\mu_1}{k_\mathrm{p}}u_2=0 \qquad \delta\leqq y\leqq H. \tag{6c}$$

The continuity of velocity and shear stress is used at $y=0$ and $y=\delta$.

3.2 The effective viscosity

The effective viscosity μ_e in the Brinkman model is a crucial parameter, which is thought to be different from the fluid viscosity and may be dependent on the fluid and the porous structure. Numerous studies have been dedicated to determining μ_e.

Brinkman [23] first used Einstein's law as an approximation, i.e., $\mu_\mathrm{e}=\mu(1+2.5\varphi)$, where $(1-\varphi)$ is the porosity, and then he recommended to set $\mu_\mathrm{e}=\mu$. According to Saffman [24], the friction term is not only proportional to the velocity but also depends on its derivative, and in that case, the comparison with the Stokes term allows for the determination of the effective viscosity: $\mu_\mathrm{e}/\mu=1/(1-2.5\varphi)$. Neale and Nader [14] established a relationship between the reduced viscosity and the structural parameter α introduced by Beavers and Joseph: $\mu_\mathrm{e}/\mu=\alpha^2$. Because α ranging from 0.1 to 4, the effective viscosity μ_e may be larger or lower than μ.

Recently, Ochoa-Tapia and Whitaker [10] derived the Brinkman equation through a volume averaging procedure and concluded that the effective viscosity concept is actually a mismatch between superficial averaged properties and intrinsic averaged properties and gave $\mu_\mathrm{e}/\mu=1/\varepsilon_\mathrm{p}$. The derivation of a correct law for the effective viscosity is still under investigation, and it probably depends on the tortuosity of the medium. Owing to the lack of suitable method to determine the exact value for the effective viscosity, the ratio $\mu_\mathrm{e}/\mu=1$ is usually applied, which is also the case in this paper.

As a parameter introduced together with the macroscopic shear terms by Brinkman, the physical nature of this effective viscosity is unclear. Actually, the Brinkman equation can be regarded as an arbitrary interpolation of the damping force and the viscous force, and the effective viscosity is also an arbitrary coefficient which can be adjusted to better fit the real situation.

3.3 The transition layer thickness

Without the knowledge of the practical structure of the interfacial porous medium and the exact expression for the varying functions of the macroscopic properties, it seems impossible to determine the thickness of the transition layer. But it may be useful to limit this layer by introducing the upper bound (interface) and the lower bound (interface). We regard the tangent of the upmost solid with porosity equal to one as the upper bound of the transition layer and the surface where the values of the macroscopic porosity firstly approach that of the homogeneous porous medium as the lower bound. As a geometrical property, the porosity can be easily measured. It is worth mentioning that the porosity here means the surface-averaged quantity as in [22].

Many authors [11,14,24,25] used a boundary layer to describe the penetration of interfacial effects into the porous medium. Here, we intend to clarify the two confusing conceptions: the boundary layer and the transition layer. The boundary layer is a zone in the homogeneous porous medium where the flow will be affected by the upper high flow field, and the velocity decreases violently to the averaged constant Darcy velocity in a distance whose length scale is normally of the order of $k^{1/2}$ [14]; however, the transition layer is the physical space necessary for the macroscopic properties varying from their values in the free-fluid region to that in the homogeneous porous medium and embraces a length scale significantly larger than that of the boundary layer. In spite of the discrepancy between these two conceptions, they are not mutually exclusive: a boundary

layer is coexistent with the transition layer if the transition layer is noticeable and specifically treated as a heterogeneous porous medium.

Some authors [20–22] have conducted experiments to investigate the transition layer thickness at a fluid–porous interface, and they found that the transition layer thickness δ is of the order of the grain diameter and much larger than the square root of the permeability, i.e., $\delta/k^{1/2} \sim 50$.

3.4 Variation function for porosity and permeability

To explore the variation of the macroscopic parameters in the heterogeneous transition layer, two sets of widely used formulations relating the permeability to porosity and the particle size for the random packing of monodisperse spheres are employed below. And here, they are constructed based on the experiment depicted in Figs. 5 and 9 in [22].

3.4.1 Linear variation function for porosity

According to the measured porosity variation in Fig. 9 in Goharzadeh et al. [22], firstly, we view the porosity variation as linear function: it decreases linearly from unity at the interface to the bulk value 0.4 with a transition layer thickness $\delta = 0.6$ cm. The porosity function is

$$\varepsilon_1(y) = -\frac{3y}{5\delta} + 1 \qquad 0 \leqq y \leqq \delta. \tag{7}$$

The intrinsic permeability k solely depends on the properties of the porous medium like pore size, shape distribution, tortuosity and porosity. Here, we just consider the properties of sphere size and porosity. The permeability function for the randomly packed monodisperse spheres is discussed below. In the Stokes assumption for a dilute bed of identical spheres, the hydraulic permeability, i.e., Stokes permeability, is obtained as [26]

$$k_1(y) = \frac{d^2}{C(1-\varepsilon)} \qquad 0 \leqq y \leqq \delta. \tag{8}$$

Here, C is a constant which is usually assigned the value 18. The inverse of the permeability function can be written as

$$\frac{1}{k_1(y)} = \frac{3Cy}{5\delta d^2} \qquad 0 \leqq y \leqq \delta. \tag{9}$$

We extend the value of $1/k_1(y)$ at $y = 0$.

3.4.2 Exponential variation function for porosity

For a monodisperse spherical packing, the Kozeny–Carman formula is also widely used in the literature. To facilitate the use of this equation in the calculation below, we use an exponential function to describe the measured porosity variation in Fig. 9 in Goharzadeh et al. [22]:

$$\varepsilon_2(y) = \varepsilon_\mathrm{p} + (\varepsilon_0 - \varepsilon_\mathrm{p}) \exp(-Ny/d) \qquad 0 \leqq y \leqq \delta, \tag{10}$$

where ε_p denotes the porosity of the homogeneous porous medium and ε_0 the porosity at the interface; d is the sphere diameter, N is a constant to fit the porosity variation with $N = 3$.

For the homogeneous porous medium, the Kozeny–Carman permeability is written as

$$k_\mathrm{CK} = \frac{\varepsilon^3 d^2}{A(1-\varepsilon)^2}, \tag{11}$$

where $A = 180$ is the Ergun constant. As the porosity ε approaches to one, the permeability of such an array of spheres is

$$k = \frac{\varepsilon^2 d^2}{B(1-\varepsilon)}. \tag{12}$$

And just like the reconstruction in [27], the expression for the variable permeability in the range of porosity $0.4 \leqq \varepsilon < 1$ is given by

$$k(y) = \frac{d^2\varepsilon^3 F(\varepsilon)}{A(1-\varepsilon)^2} \tag{13}$$

with

$$F(\varepsilon) = 1 - \exp\left[-\frac{A}{B} \times \left(\frac{1-\varepsilon}{\varepsilon}\right)\right]. \tag{14}$$

Here, $B = 18$. Eq. (13) can be degenerated into Eq. (11) or Eq. (12) as ε approaches 0.4 in the bulk medium or 1 at the interface respectively. The first approximation for the permeability function with $\varepsilon_0 = 1$ is [27]

$$k_2(y) = \frac{A10d(1-\varepsilon_\mathrm{p})}{B\varepsilon_\mathrm{p} N y} \cdot k_{\text{p-CK}}, \tag{15}$$

where $k_{\text{p-CK}}$ is the homogeneous porous medium permeability calculated using Eq. (11) based on the porosity data in Fig. 9 in [22] and $k_{\text{p-CK}} = 4.173 \times 10^{-8}\,\mathrm{m}^2$. The inverse of $k_2(y)$ for Eq. (15) is

$$\frac{1}{k_2(y)} = \frac{B\varepsilon_\mathrm{p} N y}{A10d(1-\varepsilon_\mathrm{p})} \cdot \frac{1}{k_{\text{p-CK}}} \qquad 0 \leqq y \leqq \delta. \tag{16}$$

Here, we also extend the value of $1/k_2(y)$ at $y = 0$.

4 Comparison with experiments and discussion

4.1 Numerical calculation

Free-fluid region

$$\frac{\mathrm{d}^2 u_1}{\mathrm{d}y^2} + 1 = 0 \qquad -1 \leqq y \leqq 0. \tag{17a}$$

Transition layer

$$\mu_{21}\frac{\mathrm{d}^2 u_2}{\mathrm{d}y^2} - \frac{h^2}{k(y)}u_2 + 1 = 0 \qquad 0 \leqq y \leqq \delta^*. \tag{17b}$$

Porous medium

$$\mu_{31}\frac{\mathrm{d}^2 u_3}{\mathrm{d}y^2} - \frac{1}{D_a}u_3 + 1 = 0 \qquad \delta^* \leqq y \leqq H^*. \tag{17c}$$

With boundary conditions

$$u_1(-1) = 0, \tag{18a}$$

$$u_1(0) = u_2(0) \text{ and } \mu_1 \left.\frac{\mathrm{d}u_1}{\mathrm{d}y}\right|_{y=0} = \mu_2 \left.\frac{\mathrm{d}u_2}{\mathrm{d}y}\right|_{y=0}, \tag{18b,c}$$

$$u_2(\delta^*) = u_3(\delta^*) \text{ and } \mu_2 \left.\frac{\mathrm{d}u_2}{\mathrm{d}y}\right|_{y=\delta^*} = \mu_3 \left.\frac{\mathrm{d}u_3}{\mathrm{d}y}\right|_{y=\delta^*}, \tag{18d,e}$$

$$u_3(H^*) = D_a. \tag{18f}$$

Here, δ^* and H* represent the dimensionless value corresponding to δ and H, and $\mu_{21} = \mu_2/\mu_1$, $\mu_{31} = \mu_3/\mu_1$. The general solutions of Eqs. (17a) and (17c) are

$$u_1 = -\frac{1}{2}y^2 + a_1 y + b_1, \tag{19a}$$

$$u_3 = a_3 \exp(-\sqrt{1/(\mu_{31} D_a)}y) + b_3 \exp(\sqrt{1/(\mu_{31} D_a)}y) + D_a. \tag{19c}$$

For linearly variable porosity, introducing the shorthand notation λ_1 and introducing the variable change y,

$$\lambda_1 = \left(\frac{54h^3}{5\delta d^2 \mu_{21}}\right)^{1/3}, \quad \hat{y} = \lambda_1 y, \tag{20a,b}$$

Eq. (17b) can be written as

$$\frac{\mathrm{d}^2 u_2}{\mathrm{d}\hat{y}^2} - \hat{y}u_2 + \frac{1}{\mu_{21}\lambda_1^2} = 0 \qquad 0 \leqq \hat{y} \leqq \lambda_1 \delta^*, \tag{17b*}$$

and the solution of Eq. (17b*) with a particular solution $\mathrm{Ni}(x)$ given by Nield and Kuznetsov [18] is:

$$u_2^{(1)} = a_2^{(1)}\mathrm{Ai}(\lambda_1 y) + b_2^{(1)}\mathrm{Bi}(\lambda_1 y) + \frac{\pi}{\mu_2 1}\lambda_1^2 \mathrm{Ni}(\lambda_1 y), \tag{19b}$$

where

$$\begin{aligned}
\mathrm{Ni}(x) &= \mathrm{Ai}(x)\int_0^x \mathrm{Bi}(t)\mathrm{d}(t) - \mathrm{Bi}(x)\int_0^x \mathrm{Ai}(t)\mathrm{d}(t),\\
\mathrm{Ni}'(x) &= \mathrm{Ai}'(x)\int_0^x \mathrm{Bi}(t)\mathrm{d}(t) - \mathrm{Bi}'(x)\int_0^x \mathrm{Ai}(t)\mathrm{d}(t),\\
\mathrm{Ni}(0) &= \mathrm{Ni}'(0) = 0, \mathrm{Ni}''(0) = -1/\pi.
\end{aligned} \tag{21}$$

For exponentially variable porosity, introduce the shorthand notation λ_2 and transform the variable y:

$$\lambda_2 = \left(\frac{B\varepsilon_\mathrm{p} N h^3}{A10d(1-\varepsilon_\mathrm{p})k_{\mathrm{p-CK}}\mu_{21}}\right)^{1/3}, \quad \hat{y} = \lambda_2 y. \tag{20a*,b*}$$

The same procedure is conducted, and the general solution of Eq. (17b) can be written as

$$u_2^{(2)} = a_2^{(2)}\mathrm{Ai}(\lambda_2 y) + b_2^{(2)}\mathrm{Bi}(\lambda_2 y) + \frac{\pi}{\mu_{21}\lambda_2^2}\mathrm{Ni}(\lambda_2 y). \tag{19b*}$$

The ascending series representations for $\mathrm{Ni}(x)$, $\mathrm{Ni'}(x)$ are [28]:

$$\mathrm{Ni}(x) = \mathrm{Ai}(x)\left\{\sqrt{3}\,(c_1 F_1(x) + c_2 F_2(x))\right\} - \mathrm{Bi}(x)\left\{(c_1 F_1(x) - c_2 F_2(x))\right\}, \tag{22a}$$

$$\mathrm{Ni}'(x) = \mathrm{Ai}'(x)\left\{\sqrt{3}\,(c_1 F_1(x) + c_2 F_2(x))\right\} - \mathrm{Bi}'(x)\left\{(c_1 F_1(x) - c_2 F_2(x))\right\}, \tag{22b}$$

where

$$c_1 = \mathrm{Ai}(0), \quad c_2 = \mathrm{Ai}'(0),$$
$$F_1(x) = \sum_{k=0}^{\infty} (3)^k \left(\frac{1}{3}\right)_k \frac{x^{3k+1}}{(3k+1)!}, \quad F_2(x) = \sum_{k=0}^{\infty} (3)^k (\frac{2}{3})_k \frac{x^{3k+2}}{(3k+2)!}, \tag{23}$$

where $(b)_k$ is the Pochhammer symbol,

$$(b)_k = \frac{\Gamma(b+k)}{\Gamma(b)} = b(b+1)(b+2)\cdots(b+k-1); \quad (b)_0 = 1. \tag{24}$$

Then, substituting Eqs. (19a), (19c), (19b) or (19b*) into Eqs. (18a), (18b,c), (18d,e), (18f) yields the matrix equation in which λ represents $\lambda_1$or λ_2, respectively:

$$\mathbf{Mx} = \mathbf{N},$$

$$\mathbf{M} = \begin{bmatrix} -1 & 1 & 0 & 0 & 0 & 0 \\ 0 & 1 & -\mathrm{Ai}(0) & -\mathrm{Bi}(0) & 0 & 0 \\ 1 & -\mu_{21}\lambda\mathrm{Ai}'(0) & -\mu_{21}\lambda\mathrm{Bi}'(0) & 0 & 0 & \\ 0 & 0 & \mathrm{Ai}(\lambda\delta^*) & \mathrm{Bi}(\lambda\delta^*) & -\exp\left(-\sqrt{1/(\mu_{31}D_a)}\delta^*\right) & -\exp\left(\sqrt{1/(\mu_{31}D_a)}\delta^*\right) \\ 0 & 0 & \lambda\mathrm{Ai}'(\lambda\delta^*) & \lambda\mathrm{Bi}'(\lambda\delta^*) & \frac{\mu_{32}}{\sqrt{\mu_{31}D_a}}\exp\left(-\sqrt{1/(\mu_{31}D_a)}\delta^*\right) & -\frac{\mu_{32}}{\sqrt{\mu_{31}D_a}}\exp\left(\sqrt{1/(\mu_{31}D_a)}\delta^*\right) \\ 0 & 0 & 0 & 0 & \exp\left(-\sqrt{1/(\mu_{31}D_a)}H^*\right) & \exp\left(\sqrt{1/(\mu_{31}D_a)}H^*\right) \end{bmatrix},$$

$$\mathbf{x} = \begin{bmatrix} a_1 \\ b_1 \\ a_2 \\ b_2 \\ a_3 \\ b_3 \end{bmatrix},$$

$$\mathbf{N} = \begin{bmatrix} 1/2 \\ 0 \\ 0 \\ D_a - \frac{\pi}{\mu_{21}\lambda^2}\mathrm{Ni}(\lambda\delta^*) \\ -\frac{\pi}{\mu_{21}\lambda}\mathrm{Ni}'(\lambda\delta^*) \\ 0 \end{bmatrix}.$$

After solving the above matrix equation, the velocity profile can be acquired.

4.2 Comparison and discussion

Figures 4 and 5 show the comparison between the computation results and the experimental data depicted in Fig. 5 in [22]. The parameters used in the computation are consistent with the experiment: the fluid viscosity $\mu = 42.755 \times 10^{-3}$ Pa s , the transition layer thickness $\delta = 0.6$ cm; in the transition layer, the porosity varies from 1 to 0.4 (the porosity for the below homogeneous porous packing); the permeability values are calculated using Eqs. (8) and (15), respectively; the maximum velocity in the experiment $u = 2.54$ cm/s; the pressure gradient used to match the maximum velocity is 106.88 kg/(m s)^2.

It should be noticed that the free-fluid channel in our configuration is closed, which is different from the experiment description with an open channel. Considering the velocity will reach its maximum at the top surface of the open channel in the experiment, here, the channel width for the computation is chosen as $h = 8$ cm to ensure the computed fluid velocity profile could match the experiment data at the position with maximum velocity.

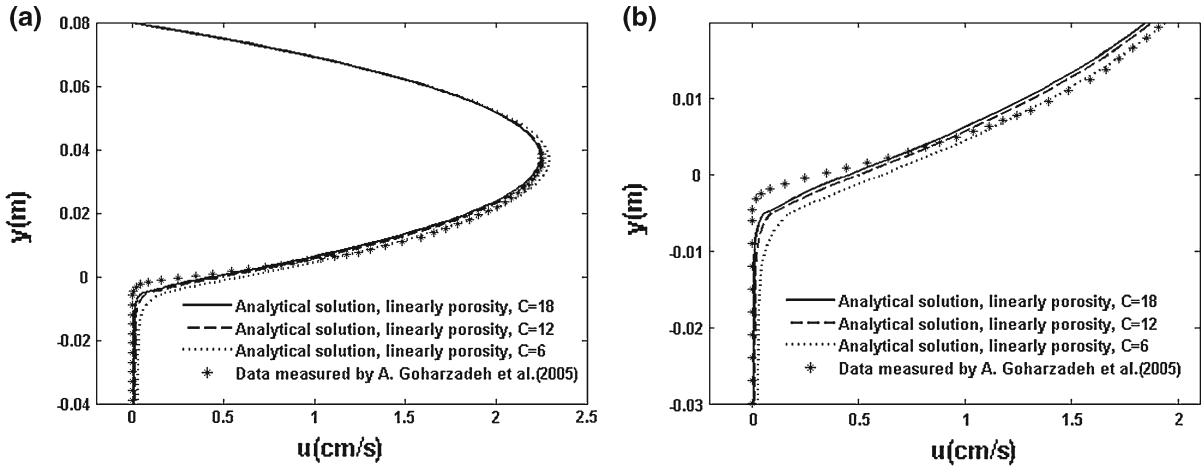

Fig. 4 A comparison between the velocity profiles acquired by the analytical solution with linear porosity and the velocity data measured by Goharzadeh et al. [22]. **a** Overall plot, **b** zoomed at the interfacial region

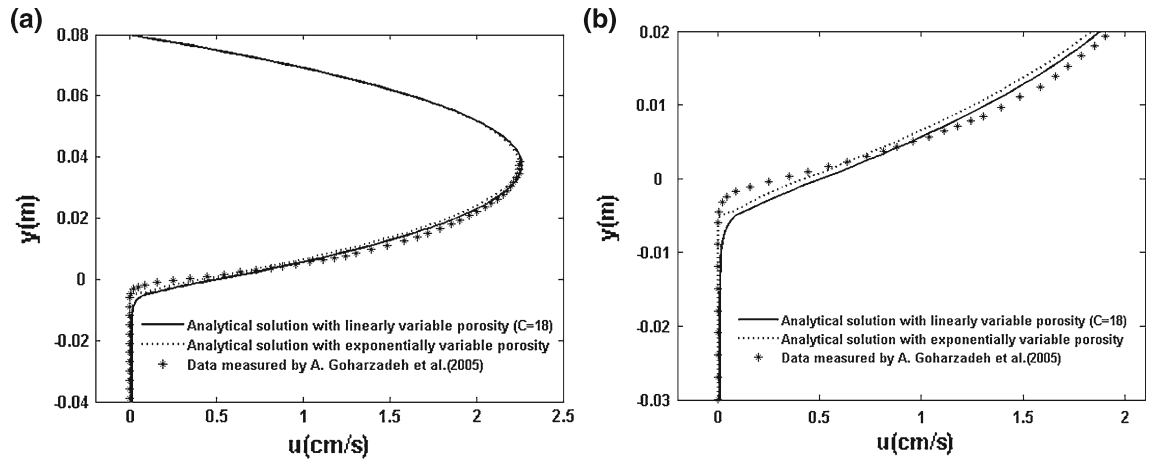

Fig. 5 A comparison between the velocity profiles acquired by the analytical solution with linear porosity ($C = 18$)/exponential porosity and the velocity data measured by Goharzadeh et al. [22]. **a** Overall plot, **b** zoomed at the interfacial region

Figure 4 shows that the computation results can well fit the experimental data, especially in the free-fluid channel. For the Stokes permeability function, as shown in Fig. 6a, the estimated permeability decreases with the increase in the parameter C if the porosity is kept constant, and this will increase the damping force due to the porous mass and cause small velocities. Thus, the analytical velocity profile with a larger value of C has a better estimation of the experimental velocity profile than that with a smaller C. In the homogeneous porous medium, the Stokes permeability function overestimates the permeability value and causes an increment of velocity in this region.

However, velocity discrepancy is illustrated in the transition layer. Two main reasons are responsible for this phenomenon. Firstly, the Brinkman equation may overestimate the velocity values, which has been reported in [25]. From Figs. 4 and 5, we can find that the velocity computed using the Brinkman equation at the fluid/porous interface is larger than that acquired by the experiment. More importantly, it is the description of the permeability variation in the transition layer that causes the discrepancy in the velocity profile: both the Stokes permeability function and the Kozeny–Carman formula cannot exactly predict the variable permeability.

Four types of permeability function are employed to compute the velocity profiles as shown in Fig. 6a. In the transition layer, the permeability considering exponential porosity possesses the lowest values. With the increase in the constant C, the transition layer permeability considering linear permeability decreases. For each type, the permeability will reach an infinitely large value at the fluid/porous interface. And then, it will decrease sharply into a small value at the lowest level of the transition layer.

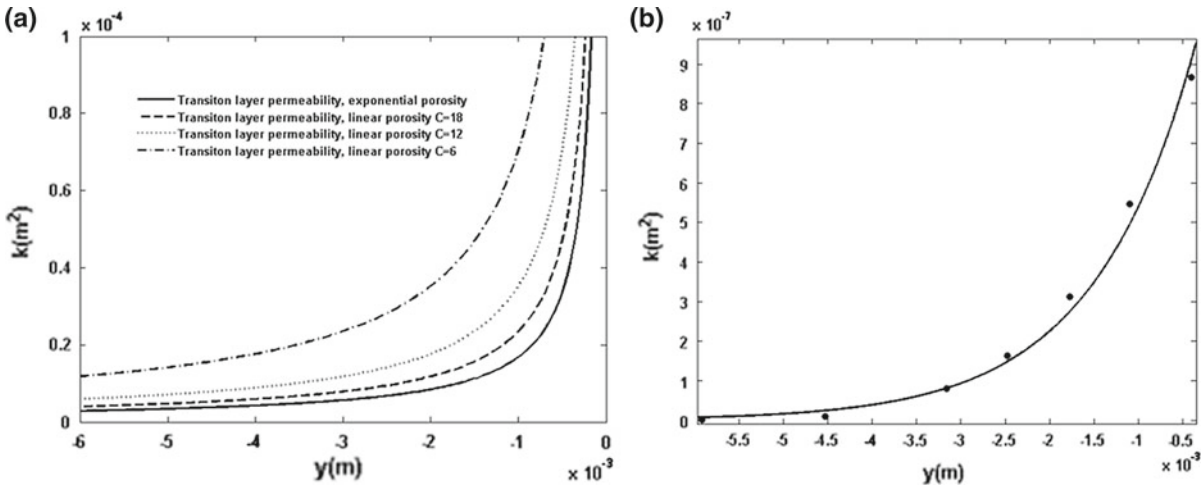

Fig. 6 **a** Permeability variations in the transition layer, **b** the calculated transition layer permeability corresponding to the experiment conducted by Goharzadeh et al. [22]

In Fig. 6b, the calculated transition layer permeability corresponding to the experiment conducted by Goharzadeh et al. [22] is shown, and the variation of the permeability in the transition layer is obtained from the measured velocity field and by using Eq. (25):

$$k(y) = \frac{\mu u}{\mu_{\mathrm{e}} \frac{\mathrm{d}^2 u}{\mathrm{d}y^2} - \frac{\mathrm{d}p}{\mathrm{d}x}}. \tag{25}$$

Comparing Figs. 6a and b, we can find the actual permeability is two orders of magnitude smaller than that predicted by the Stokes permeability function or the Kozeny–Carman formula, which causes the large velocity discrepancy in the transition layer. For the specific experiment of Goharzadeh et al. [22], we fit the calculated data with the exponential formula and the expression of the fitting function is:

$$k(y) = 1.296 \times 10^{-6} \exp(876.3y) \qquad -\delta \leqq y \leqq 0. \tag{26}$$

According to the above discussion, both the Stokes permeability function and the Kozeny–Carman formula overestimate the gradual permeability variation in the transition layer. Although, as a permeability forecasting function for the monodisperse spherical packing bed with uniform porosity, the Kozeny–Carman formula can precisely predict the permeability in the homogeneous porous medium, it is incapable of describing the permeability variation in the non-homogeneous porous bed.

5 Conclusion

In this paper, the fluid–porous coupling flow problem is studied analytically. Firstly, comparison between the single-domain approach and the widely used two-domain approach is conducted to address the necessity of specifically modeling the change in macroscopic parameters along the transition region. The three-layer model consists of a free-fluid channel, a heterogeneous transition layer characterized by variable macroscopic properties and a homogeneous porous medium. Special focus is put on the macroscopic properties of the transition layer. Two specific permeability functions are employed to express the permeability variation. Then, analytical expressions for velocity profiles in each layer are given involving the use of Airy functions. After comparing the analytical solution with the experiment data measured by Goharzadeh et al. [22], a good fit between the computation results and the experimental data especially in the free-fluid channel is shown. However, a large velocity discrepancy in the transition layer is illustrated.

Through this research, we find that although the well-known Kozeny–Carman formula can predict the permeability precisely for the monodisperse spherical packing bed, it will amplify the transition layer permeability variation in the transition layer. A similar conclusion can be reached for the Stokes permeability function. The

exact description of the permeability in the transition layer is a vital factor that influences the matching result. Further research is needed to study other ways of depicting the variable properties in the transition layer. Moreover, detailed laboratory experiments are indispensible, and a precise permeability forecasting function is needed to model the gradual change of permeability along the transition layer region.

Acknowledgments This work was supported by the National Basic Research Program of China ("973" Program) (Grant No. 2011CB201004), the Important National Science and Technology Project of China (Grant No. 2011ZX05014-005-003HZ), the National Natural Science Foundation of China (Grant No. 11102237) and the Fundamental Research Funds for the Central Universities (Grant No. 11CX06026A, 14CX02042A)

References

1. Jamet, D., Chandesris, M., Goyeau, B.: On the equivalence of the discontinuous one- and two-domain approaches for modeling of transport phenomena at a fluid–porous interface. Transp. Porous Med. **78**, 403 (2009)
2. Goyeau, B., Lhuillier, D., Gobin, D.: Momentum transport at a fluid–porous interface. Int. J. Heat Mass Transf. **46**, 4071 (2003)
3. Beckermann, C., Viskanta, R., Ramadhyani S., R.: Natural convection in vertical enclosures containing simultaneously fluid and porous layers. J. Fluid Mech. **186**, 257 (1988)
4. Beckermann, C., Ramadhyani, S., Viskanta, R.: Natural convection flow and heat transfer between a fluid layer and a porous layer inside a rectangular enclosure. J. Heat Transf.-T ASME **109**, 363 (1987)
5. Song, M., Viskanta, R.: Natural convection flow and heat transfer within a rectangular enclosure containing a vertical porous layer. Int. J. Heat Mass Transf. **37**, 2425 (1994)
6. Nield, D., Bejan, A.: Convection in Porous Media. Springer, New York (1992)
7. Discacciati, M.: Domain decomposition methods for the coupling of surface and groundwater flows. Ph.D. thesis, Ecole Polytechnique Fédérale de Lausanne, Switzerland (2004)
8. Beavers, G., Joseph, D.D.: Boundary conditions at a naturally permeable wall. J. Fluid Mech. **30**, 197 (1967)
9. Alloui, Z., Vasseur, P.: Convection in superposed fluid and porous layers. Acta Mech. **214**, 245–260 (2010)
10. Ochoa-Tapia, J.A., Whitaker, S.: Momentum-transfer at the boundary between a porous-medium and a homogeneous fluid: 1. Theoretical development. Int. J. Heat Mass Transf. **38**, 2635–2646 (1995)
11. Ochoa-Tapia, J.A., Whitaker, S.: Momentum transfer at the boundary between a porous medium and a homogeneous fluid. II. Comparison with experiment. Int. J. Heat Mass Transf. **38**, 2647–2655 (1995)
12. Chandesris, M., Jamet, D.: Boundary conditions at a planar fluid–porous interface for a Poiseuille flow. Int. J. Heat Mass Transf. **49**, 2137 (2006)
13. Duman, T., Shavit, U.: An apparent interface location as a tool to solve the porous interface flow problem. Transp. Porous Med. **78**, 509 (2009)
14. Neale, G., Nader, W.: Practical significance of Brinkman's extension of Darcy's law: coupled parallel flows within a channel and a bounding porous medium. Gun. J. Chem. Eng. **52**, 415478 (1974)
15. Chandesris, M., Jamet, D.: Boundary conditions at a fluid–porous interface: an a priori estimation of the stress jump coefficients. Int. J. Heat Mass Transf. **50**, 3422 (2007)
16. Hill, A.A., Straughan, B.: Poiseuille flow in a fluid overlying a porous medium. J. Fluid Mech. **603**, 137 (2008)
17. Hill, A.A.: Instability of Poiseuille flow in a fluid overlying a glass bead packed porous layer. Acta Mech. **206**, 95 (2009)
18. Nield, D.A., Kuznetsov, A.V.: The effect of a transition layer between a fluid and a porous medium: shear flow in a channel. Transp. Porous Med. **78**, 477 (2009)
19. Duman, T., Shavit, U.: A solution of the laminar flow for a gradual transition between porous and fluid domains. Water Resour. Res. **46**, W09517 (2010). doi:10.1029/2009WR008393
20. Goharzadeh, A., Saidi, A., Wang, D., Merzkirch, W., Khalili, A.: An experimental investigation of the Brinkman layer thickness at a fluidporous interface. In: Meier, G.E.A., Sreenivasan, K.R. One Hundred Years Boundary Layer Research, Springer, New York (2005)
21. Morad, M.R., Khalili, A.: Transition layer thickness in a fluid-porous medium of multi-sized spherical beads. Exp. Fluids **46**, 323 (2009)
22. Goharzadeh, A., Khalili, A., Jorgensen, B.B.: Transition layer at a fluid–porous interface. Phys. Fluids **17**, 057102 (2005)
23. Brinkman, H.C.: A calculation of the viscous force exerted by a flowing fluid on a dense swarm of particles. Appl. Sci. Res. A **1**, 27 (1947)
24. Saffman, P.G.: On the boundary condition at the interface of a porous medium. Stud. Appl. Math. **50**, 93 (1971)
25. Sahraoui, M., Kaviany, M.: Slip and no-slip velocity boundary conditions at interface of porous, plain media. Int. J. Heat Mass Transf. **35**, 927 (1992)
26. Torquato, S.: Random Heterogeneous Materials: Microstructure and Macroscopic Properties. Springer, New York (2002)
27. Hsu, C.T., Cheng, P.: A singular perturbation solution for Couette flow over a semi-infinite porous bed. J. Fluids Eng. **113**, 137 (1991)
28. Vallée, O., Soares, M.: Airy Functions and Applications to Physics. World Scientific, London (2004)